Research on Anti-Jamming Technology of Chaotic Composite Short Range Detection System Based on Underdetermined Signal Separation and Spectral Analysis

DONGXU WEI[1,2], **SHUNING ZHANG**[1], **SI CHEN**[1], **HUICHANG ZHAO**[1], **AND LINGZHI ZHU**[1]

[1]School of Electronic & Optical Engineering, Nanjing University of Science and Technology, Nanjing 210094, China
[2]School of Physics and Electronic Electrical Engineering, Huaiyin Normal University, Huai'an 223300, China

Corresponding author: Shuning Zhang (shuningzhangnjust@163.com)

ABSTRACT The chaotic phase-modulated linear frequency modulation short-range detection system (CPLF-SrDS) is a new type of composite detection system. Compared with traditional methods, it benefits from the short-term randomness and long-term certainty of chaos and is more powerful in determining the distance. To design such a system, the key problem lies in robustly recovering the echo signal against externally suppressed interferences. Combining 4th-order cumulant and joint diagonalization, this paper first develops a new signal separation approach to realize an underdetermined separation of the echo signal and an interference signal from their mixture. Then, both bispectrum analysis and singular spectrum analysis are adapted to analyze the separated signals and extract their characteristic parameters. Furthermore, the GA-BP network is utilized to classify the echo and interference signals. Finally, the anti-interference analysis of this CPLF-SrDS is realized. The experimental results show the effectiveness of the proposed method in the presence of externally suppressed amplitude modulation (AM) interference and frequency modulation (FM) interference.

INDEX TERMS Composite detection system, robust signal separation, anti-jamming technology, bispectrum analysis, singular spectrum analysis.

I. INTRODUCTION

A distinctive feature of modern local warfare is information-ization. Radio proximity detection has become an indispensable element of information warfare. Recently, real battlefield environments have made more stringent requirements for the anti-jamming performance of a radio proximity detection system (RPDS), especially for low-altitude aircraft, sea-skimming missiles, ground fire control radar and other target detection systems [1]–[3]. Among different types of RPDS, the CPLF-SrDS exploits the short-term randomness and long-term certainty of chaos, and has strong ability to determine the distance. Due to the advantages over traditional composite detection systems, it has become an emerging topic in current research. However, the emergence of CPLF-SrDS also gives rise to developments of related interference techniques

aiming to affect the normal work of the system. Thus, it is of practical significance to design an effective anti-interference method to ensure the normal operations of the detection system [4], [5].

Due to the interference, one can only observe a mixture of the echo signal and the interference signal in a short-range detection system (SrDS). Then, it is a premise of the anti-interference analysis to effectively separate the mixed signals. Although researches on multi-component signal separation have made some progress, most of them focus on separating multi-component signals under positive and over-determined conditions. The difference is that, the problem we encounter is an under-determined signal separation. Since each component generally has a relatively complex time-frequency distribution, its frequency domain has a wide bandwidth, making the spectrum of the mixture generally inter-leaved. That is, such multi-component signals overlap each other in the time domain, the frequency domain and the

---

The associate editor coordinating the review of this manuscript and approving it for publication was Jinming Wen.

time-frequency plane, which makes it highly complicated and challenging to separate them from each other.

The under-determined signal separation problem has attracted much attention. In [6], by exploiting the signal sparsity characteristics, the underdetermined blind source is separated by searching for the method with the largest sparsity solution. Literature [7] proposed to estimate the hybrid matrix by clustering method for signal separation. A signal separation method based on the Bayesian method with the greatest expectation was proposed in [8]. Literatures [9], [10] solve the underdetermined blind source separation problem through non-negative matrix factorization and finite sub-symbol set. A subspace projection based algorithm was developed in [11]. Since some of the above methods assume the source signal to satisfy some sparsity conditions, they are impractical to solve the blind separation problem of the radar signal under the condition of time domain and frequency domain aliasing and insufficient sparseness. Some of the researches have difficulties in recovering the source signals when the number of source signals at any time-frequency point is smaller than some set value. In view of the above deficiencies, this paper proposes an underdetermined blind signal separation method based on 4th-order cumulant and joint diagonalization.

It is also necessary to identify the separated signals to achieve anti-interference of the system. In [12], the fuzzy function is used to study the anti-interference performance of FM continuous wave fuze. The literatures [13], [14] used the processing gain method to analyze the anti-interference of pseudo-code composite fuze. The literatures [15], [16] adopted the signal-to-interference ratio gain method to analyze the anti-interference performance of UWB fuze and pulse Doppler fuze. At present, there is little research on the anti-interference of the chaotic composite system detection system. Moreover, when the correlation parameters of the echo signal and the interference signal are close, it is difficult to classify the echo and interference.

Literature [17] proposed a novel anti-jamming approach based on Singular Spectrum Analysis, and realized anti-spoofing interference analysis of the system. The literatures [18] used deep belief network and bispectra diagonal slice realized the signal recognition of the low probability of intercept radar. In [19], singular spectrum analysis has been used for the effective feature extraction in hyperspectral imaging. In this paper, the bispectrum analysis and singular spectrum analysis will be utilized to classify of echo and interference to achieve anti-interference of the system. Compared with the traditional method, it can better mine the deep features of the signal and realize the classification and recognition of the signal.

In this paper, for the characteristic parameters set of echo and interference, the genetic algorithm is used to optimize the initial weight and threshold of BP neural network. Then BP algorithm is applied to fine tune the network in this solution space to search for the optimal solution. Compared with the traditional BP algorithm, this algorithm replaces
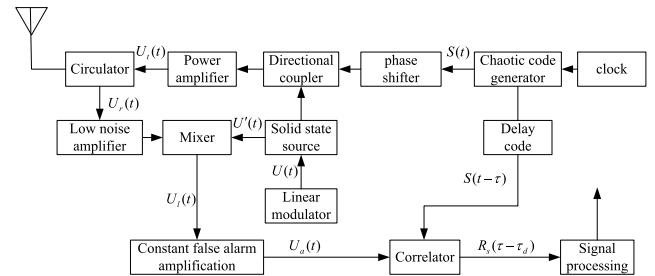

FIGURE 1. Compound detection block diagram of the proposed CPLF-SrDS.

the random selection of the traditional initial weights, which speeds up the learning speed of the system and improves the approximation ability in the whole learning process.

The rest of this paper is organized as follows. Section II expounds the working principle of CPLF-SrDS. Section III realizes the underdetermined separation of echo and two kinds of interferences, which is based on the 4th-order cumulant and joint diagonalization method. In Section IV, the singular spectrum analysis is carried out on the separated signal, and the singular spectrum entropy is extracted. In Section V, bispectral analysis method is utilized for the separated signal, and two characteristic parameters (i.e., bispectral slice convexity and bispectral peak entropy) are proposed. Section VI adopts the GA-BP network to classify the echo and interference.

II. PRINCIPLE OF SHORT-RANGE DETECTION
The block diagram of the proposed CPLF-SrDS is shown in Fig. 1. It consists of a linear modulator, a chaotic code generator, an oscillator, a phase modulator, a correlator, and an execution stage.

As shown in Fig. 1, the sawtooth signal generated by the linear modulator first enters the oscillator, producing a modulated chirp signal $U(t)$. Then, $S(t)$ generated by the chaotic code generator is phase-modulated in the phase modulator. Next, the modulated signal $U_t(t)$ is radiated into the space by the transmitting antenna after passing through the coupler and the power amplifier. After the probe signal $U_t(t)$ encountering the target, a part of the energy is reflected and received by the receiving antenna. The echo signal is mixed with the chirp signal $U_l(t)$ from the transmitter oscillator, and a chaotic code delay code carrying the target distance information is obtained at the output of the mixer. After the constant false alarm being amplified, the correlation code set in the correlator is related to the signal, thereby achieving the purpose of the distance.

III. UNDERDETERMINED SIGNAL SEPARATION
The transmission signal of the CPLF-SrDS is often interfered by the signal transmitted by the jammer. Since the echo signal and the interference signal are mixed together, it seriously affects the normal operations of the system. To conduct anti-jamming technology research of such an institutional system, it is necessary to perform effective separations on the mixed signal. However, there is only one antenna for traditional

short-range detection which receives the echo signal, and the echo signal tends to be mixed with various interferences. Thus, the separation of the echo and the interference signal is an under-determination problem.

Joint approximation diagonalization based signal separation is an important method used in recent years. However, when the signal-to-noise ratio is low, the separation performance is far from satisfactory. For promising signal separation, we first compute the 4th-order cumulant of the signal and then use the 4th-order cumulant slice to perform the joint diagonalization process. This method can improve the similarity of the waveforms after signal separation and recovery under low signal-to-noise ratio. The details are given as follows.

A. SIGNAL 4TH -ORDER CUMULANT SOLUTION

It is known that based on the correlation matrix, more information of the observation signals can be obtained. Further, high-order cumulants can generate even more information of the observation signals and have an inhibitory effect on Gaussian noise. As shown in [20], [21], the 4th-order cumulant of the signal contains most of the valid information of the source signal and is robust to noise signals. This subsection proposes to combine joint diagonalization with high-order cumulant for signal separation.

The 4th-order cumulant is a 3-D matrix, and the dimension of the matrix is determined by the amount of delay. In order to expand the obtained observation signal, and remove the colored noise at the same time, we use the matrix slice as a reference signal.

Taking the mixed observation signals of three independent sources for example, it is assumed that the independent source signal is $s_i = \sum_{u=1}^{U_i} b_{iu} e^{j(\omega_{iu} + \varphi_{iu})}$, where: b_{iu} is the amplitude of a certain frequency in the independent source, u is the frequency serial number, i is the independent source number, $i = 1, 2, 3$; and ω_{iu} is the frequency component; φ_{iu} is the phase corresponding to the frequency component; U_i is the number of frequency components included in the i-th independent source.

The original three independent sources s_1, s_2, s_3, assuming a mixed matrix $A = \begin{bmatrix} a_{11} & a_{12} & a_{13} \\ a_{21} & a_{22} & a_{23} \end{bmatrix}$, the mixed observation signals are calculated as:

$$X = AS = \begin{bmatrix} a_{11} & a_{12} & a_{13} \\ a_{21} & a_{22} & a_{23} \end{bmatrix} [s_1, s_2, s_3]^T \quad (1)$$

The formula for calculating the cumulative amount of observed signals is:

$$
\begin{aligned}
C_{ij} = &\, E[x_i(t), x_i(t+\tau_1), x_j(t+\tau_2), x_j(t+\tau_3)] \\
&- E[x_i(t), x_i(t+\tau_1)]E[x_j(t+\tau_2), x_j(t+\tau_3)] \\
&- E[x_i(t), x_i(t+\tau_2)]E[x_j(t+\tau_1), x_j(t+\tau_3)] \\
&- E[x_i(t), x_i(t+\tau_3)]E[x_j(t+\tau_1), x_j(t+\tau_2)] \quad (2)
\end{aligned}
$$

where: x_i, x_j are two different observation signal, τ_1, τ_2 and τ_3 are the delay values of x_1, x_2 and x_3; $E[\cdot]$ denotes the expectation operator.

Then, slices of the mutual 4th-order cumulant of two observation signals can be calculated as follows:

$$
\begin{aligned}
C_{xy} = &\, -\frac{1}{8} \sum_{i=1}^{3} \sum_{u=1}^{U_i} (a_{1i}a_{2i})^2 b_{iu}^4 e^{j\omega_{iu}(-\tau_1+\tau_2+\tau_3)} \\
&- \frac{1}{8} \sum_{i=1}^{3} \sum_{u=1}^{U_i} (a_{1i}a_{2i})^2 b_{iu}^4 \exp[j\omega_{iu}(\tau_1 - \tau_2 + \tau_3)] \\
&- \frac{1}{8} \sum_{i=1}^{3} \sum_{u=1}^{U_i} (a_{1i}a_{2i})^2 b_{iu}^4 \exp[j\omega_{iu}(\tau_1 + \tau_2 - \tau_3)] \quad (3)
\end{aligned}
$$

To reduce the complexity of 4th-order cumulant estimation in engineering implementation, one does not need computing all delay matrices. Regarding the following three kinds of slice forms, only the cumulant slice feature needs to contain the source signal features, and the hybrid matrix can be reversible. Based on Eq. (3), the reversibility of the mixed matrix of the observed signals in different slice forms is discussed.

a. When $\tau_1 = \tau_2 = \tau_3 = \tau \neq 0$,

$$C_{xy} = -\frac{3}{8} \sum_{i=1}^{3} \sum_{u=1}^{U_h} (a_{1i}a_{2i})^2 b_{iu}^3 s_i(\tau) \quad (4)$$

b. When $\tau_1 = 0, \tau_2 = \tau_3 \neq 0$ or $\tau_2 = 0, \tau_1 = \tau_3 \neq 0$ or $\tau_3 = 0, \tau_1 = \tau_2 \neq 0$,

$$C_{xy} = -\frac{1}{8} \sum_{i=1}^{3} \sum_{u=1}^{U_i} (a_{1i}a_{2i})^2 b_{iu}^3 s_i(\tau) - \frac{2}{8} \sum_{i=1}^{3} \sum_{u=1}^{U_h} (a_{1i}a_{2i})^2 b_{iu}^4 \quad (5)$$

c. When $\tau_1 \neq 0, \tau_2 = \tau_3 = 0$,

$$real(C_{xy}) = -\frac{3}{8} \sum_{i=1}^{3} \sum_{u=1}^{U_i} (a_{1i}a_{2i})^2 b_{iu}^3 real(s_i(\tau)) \quad (6)$$

where $real(\cdot)$ is the real part in the formula.

Eq. (6) contains a large DC component. When selecting a slice, it is necessary to consider the mean and then the cumulative matrix. The slice matrix formed by the mutual 4th-order cumulant of Eqs. (4)-(6) can expand the number of observation signals, and the a, c slice retains the frequency characteristics of the source information, and the slice selection space of c is large. In order to make the amplitude difference of each observed signal of the mutual cumulant amount relatively small, the multi-path observation signal is generated in the slice state of c, namely:

$$X_1 = -\frac{3}{8} \sum_{i=1}^{3} \sum_{u=1}^{U_i} (a_{1i})^3 a_{2i} b_{iu}^3 s_i(\tau) \quad (7)$$

$$X_2 = -\frac{3}{8} \sum_{i=1}^{3} \sum_{u=1}^{U_i} (a_{1i}a_{2i})^2 b_{iu}^3 s_i(\tau) \quad (8)$$

$$X_3 = -\frac{3}{8} \sum_{i=1}^{3} \sum_{u=1}^{U_i} a_{1i}(a_{2i})^3 b_{iu}^3 s_i(\tau) \quad (9)$$

The new 3-way observation signal (X_1, X_2, X_3) formed above retains the frequency characteristics of independent source s_i, and forms a new matrix A_R that satisfies reversibility. That is, A_R has diagonalizable characteristics.

B. JOINT DIAGONALIZATION SIGNAL SEPARATION

1) PRETREATMENT

In order to effectively achieve multiple signal separation, it is necessary to preprocess the 4th-order cumulant slice of the observed signal. Pretreatment can be divided into two stages of centralization and whitening [22], [23]. The centralization process makes the 4th-order cumulant slice to be zero; and the whitening process refers to seeking the whitened matrix $Q \in C^{N \times M}$ such that the signal covariance matrix after whitening is a unit matrix.

$$Q = E^{-1/2}V^T \tag{10}$$

$$Z(t) = QX(t) = QAS(t) = US(t) \tag{11}$$

$$R_{ZZ} = E[Z(t)Z^H(t)] = I \tag{12}$$

where: E is the diagonal matrix storing N largest eigenvalues (sorted from largest to smallest) of the correlation matrix R_{XX} of the observation signal $X(t)$; V is a matrix composed of the corresponding eigenvectors of the N eigenvalues, by using Eq. (12) substituting Eq. (13) to calculate that U is an orthogonal matrix. However, the above analysis dose not consider the noise which cannot be ignored in real environments. Therefore, a noise compensation method is proposed. By subtracting the noise kinetic rate σ^2 during whitening, σ^2 can be estimated from the signal covariance matrix. Note the noise whitening matrix is:

$$Q = (E - \sigma^2 I)^{-1/2}V^T \tag{13}$$

Then the spatial time-frequency distribution matrix of the whitened signal can be approximated by:

$$D_{ZZ}(t,f) = QD_{XX}(t,f)Q^H = U \times D_{SS}(t,f) \times U^H \tag{14}$$

It can be seen from the above formula that when the frequency point is the time-frequency point corresponding to the signal self-term, the time-frequency distribution matrix $D_{SS}(t,f)$ of the source signal is a diagonal matrix. Then, the matrix U can be obtained by diagonalizing the time-frequency matrix of the self-term time-frequency point. Therefore the key to the separation of the source signals is the selection of the time-frequency points of the signal.

2) NON-ORTHOGONAL JOINT DIAGONALIZATION

Blind source separation requires that the source signals are independent of each other. The whitening process can greatly reduce the correlation between the mixed signals and compress the information through dimensionality reduction. Although noise is compensated, it is inevitable that noise errors are accumulated, the matrix U obtained after whitening is not a standard orthogonal matrix, so the traditional diagonalization method cannot get a more accurate separation

matrix. The advantage of the non-orthogonal joint diagonalization algorithm is that the diagonalization matrix U are not limited to be orthogonal (see ACDC (Alternating Columns Diagonal Centers) [24], [25]). First, we construct the objective function:

$$R_{LS}(U, \Lambda_1, \Lambda_2, \cdots \Lambda_k) = \sum_{k=1}^{K} w_k \left\| D_k - U \Lambda_k U^H \right\|_F^2 \tag{15}$$

where: D_k is the spatial time-frequency distribution matrix of the selected kth time-frequency point; Λ_k is the diagonal matrix; w_k is the weighting coefficient. The steps of computing U is briefly described as follows:

Step 1: Select a set of spatial time-frequency distribution matrix sets $\{D_k\}$, initialize the matrix U and matrix set $\{\Lambda_k\}$, and set it as an identity matrix.

Step 2: AC (Alternating Columns) stage: Randomly select one of the column vectors of U as a variable, and substitute the equation (15) to obtain the minimum value of the objective function R_{LS}.

Step 3: DC (Diagonal Centers) stage: Update the diagonal matrix Λ_k according to the AC phase while keeping the matrix U unchanged, and use the Eq. (15) to minimize the objective function.

Step 4: The two phases of AC-DC are alternately iterated until the objective function reaches the desired value. When the value of the objective function satisfies the expected requirement, the matrix U is the separated matrix at the time.

C. UNDERDETERMINED SIGNAL SEPARATION EXPERIMENT

The chaotic phase-modulated sawtooth amplitude modulation signal is selected as the system echo, while the sawtooth frequency modulation signal and the sinusoidal frequency modulation signal are selected as two different interferences. For the echo of the CPLF-SrDS, the chaotic sequence is generated by logistic mapping, the symbol width of the chaotic code is 50ns, the carrier frequency is 5GHz, the modulation frequency is 5kHz, and the modulation bandwidth is 100MHz. For the sawtooth AM interference, the carrier frequency is 5GHz, the modulation frequency is 5kHz, and the modulation bandwidth is 100MHz. For the sinusoidal FM interference, the carrier frequency is 5GHz, the modulation frequency is 5kHz, and the frequency offset is 20MHz. Several signals are aliased in both the time and the frequency domain, leading to a more complicated composite form. Using the above three source signals, underdetermined signal separation experiments are conducted under different signal-to-noise ratio (SNR) conditions. To better verify the separation performances, we add Gaussian white noise of a certain SNR in the mixing process. Three generated source signals are shown in Fig. 2-4, respectively.

Fig. 5 plots the noisy mixed signal with SNR = 10dB. Fig.6-8 show the recovered signal with SNR = 10dB. As can be seen, the source signal and the recovered signal are substantially overlapping, except that there is a slight

TABLE 1. Signal recovery similarity under different SNR conditions.

SNR	The recovery signal similarity of echo	The recovery signal similarity of sawtooth AM	The recovery signal similarity of sinusoidal FM
0	0.7172	0.6333	0.6331
3	0.7627	0.6976	0.7419
4	0.8021	0.7270	0.7775
5	0.8591	0.8066	0.8582
10	0.9748	0.8879	0.9740
20	0.9970	0.9717	0.9972
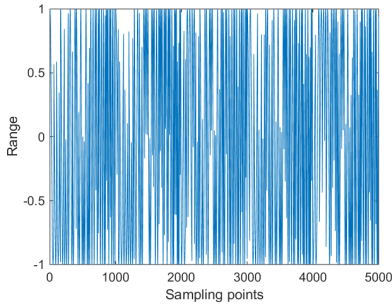
FIGURE 2. Detection echo signal.
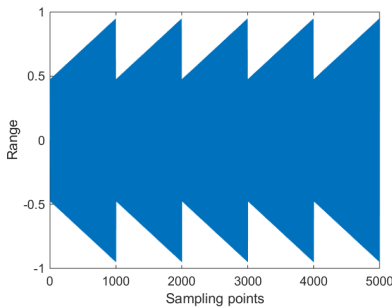
FIGURE 3. Sawtooth AM interference signal.
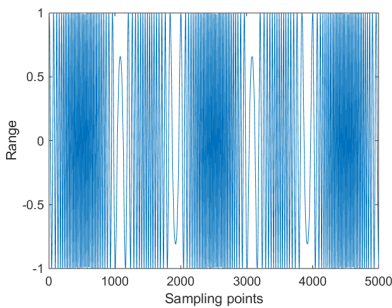
FIGURE 4. Sinusoidal FM interference signal.

FIGURE 5. Mixed signal.

FIGURE 6. The recovery signal of detection echo.

FIGURE 7. The recovery signal sawtooth AM interference.

FIGURE 8. The recovery signal of sinusoidal FM interference.

difference at some of the amplitude points. Then, it is verified that the proposed separation method can promisingly achieve the separation of underdetermined signals.

Given two waveforms $y_i(t)$ and $s_i(t)$, the following metric is used to measure their similarities:

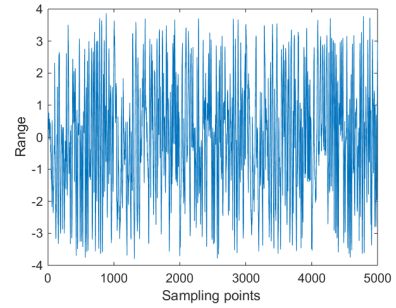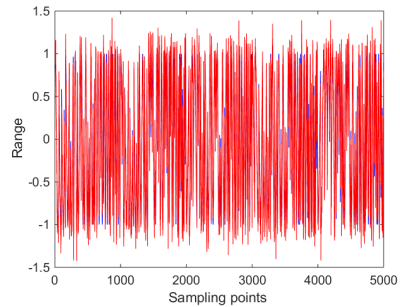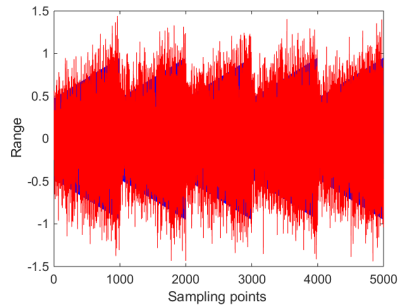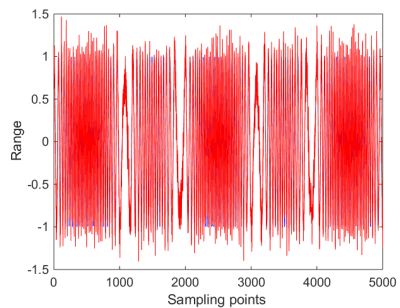$$\rho_{ij} = \rho(y_i, s_j) = \frac{|E[y_i(t)s_j(t)]|}{\sqrt{|E[y_i^2(t)]E[s_j^2(t)]|}} \qquad (16)$$

The closer ρ_{ij} is to 1, the better the waveform recovery is. If $\rho_{ij} \approx 0$, the signal is almost dissimilar. Letting $y_i(t)$ and $s_i(t)$ denote the separation signal and the source signal respectively, their similarity is measured according to Eq. (16). Next, the similarity is used to evaluate the effectiveness of the proposed separation method.
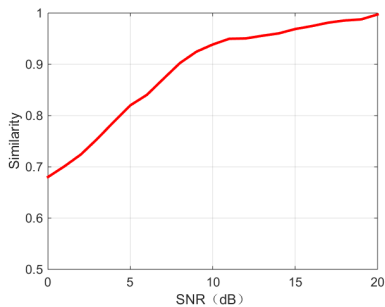
FIGURE 9. The restoring waveform similarity with different SNR.

FIGURE 10. The distribution of detection echo singular value.

To measure the anti-noise performance, we carry out multiple simulation experiments under different settings and report the averaged similarity values. The plot of the averaged similarity value versus the SNR is shown in Fig. 9. It can be seen that when the SNR is greater than 8dB, the separation effect is satisfactory with the averaged similarity greater than 0.9; even if the signal-to-noise ratio is 0 dB, the waveform similarity can reach 0.66.

IV. SINGULAR SPECTRUM ANYALYSIS

In this section, we will combine the singular spectrum analysis and bispectrum analysis methods to extract features of detection echoes and different interference signals.

A. SINGULAR VALUE DECOMPOSITION

Singular spectrum analysis is popular a time series analysis method. The signal is reconstructed in phase space with delay coordinates [17], [26], [27]. Let $x = [x_1, x_2, \cdots, x_n] \in R^N$ be a vector signal. With a window size $L \in [1, N/2]$, the trajectory matrix X of signal is constructed as follows:

$$X = \begin{bmatrix} x_1 & x_2 & \cdots & x_K \\ x_2 & x_3 & \cdots & x_{K+1} \\ \vdots & \vdots & \ddots & \vdots \\ x_L & x_{L+1} & \cdots & x_N \end{bmatrix} = [X_1, X_2, \cdots X_i] \quad (17)$$

where $X_i = [x_i, x_{i+1}, \cdots x_{i+L-1}]^T \in R^N$, $i = 1, 2, \cdots, K$, $K = N - L + 1$.

Using eigenvalue decomposition of matrix $Y = XX^T$, the eigenvalues of matrix Y and their corresponding eigenvectors are $(\lambda_1 \geq \lambda_2 \geq \cdots \geq \lambda_L)$ and $(U_1, U_2, \cdots U_L)$. Then the singular value decomposition (SVD) of trace matrix X can be given as follows:

$$Y = U\Sigma V^T, \quad \Sigma = \begin{pmatrix} S & 0 \\ 0 & 0 \end{pmatrix},$$

$$S = diag(\sqrt{\lambda_1}, \sqrt{\lambda_2} \cdots \sqrt{\lambda_r})$$

$$X = P_1 + P_2 + \cdots + P_L \quad (18)$$

where matrices $U = (u_1, \cdots, u_L)$, $V = (v_1, \cdots, v_L)$ with column vectors $v_i = X^T u_i / \sqrt{\lambda_i}$, matrix $P_i = \sqrt{\lambda_i} u_i v_i^T$ is an elementary matrix, $\sqrt{\lambda_i}$ is the i-th largest singular value the trace matrix X, u_i and v_i are the left and right singular vectors with $\sqrt{\lambda_i}$ respectively.
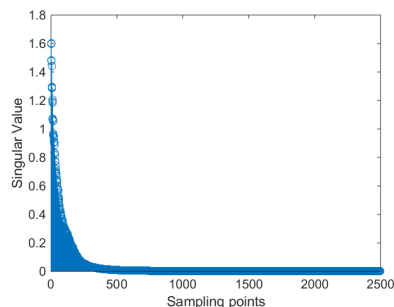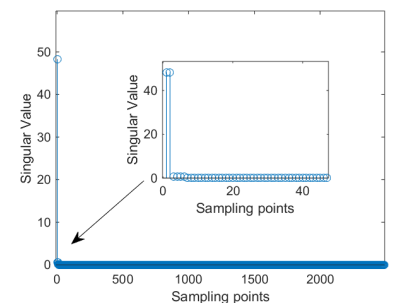

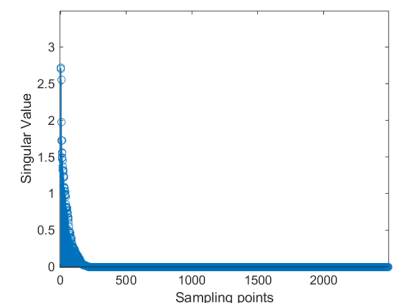**FIGURE 11.** The distribution of sawtooth AM interference singular value.

FIGURE 12. The distribution of sinusoidal FM interference singular value.

Information of the source signal can be well reflected through the rank (i.e., the number of non-zero singular values) and the amplitude distribution of singular values of the trace matrix X. Next, we will analyze the singular values of three source signals, i.e., the chaotic phase-modulated sawtooth frequency modulated signal, the sawtooth amplitude modulation interference signal, and the sinusoidal frequency modulation interference signal.

Fig. 10-12 show the singular value distribution of the detected echo and two different interferences. It is found that the singular value distribution of sawtooth amplitude modulation interference and system detection echo are clearly different. The rank corresponding to the detection echo signal is significantly larger than that of amplitude modulation interference. The trace matrix of amplitude modulation interference is very low-rank, i.e., most of the singular values are zero. On the contrary, the singular value of the detected echo signal tend to decrease slowly. For sinusoidal frequency

modulation interference, the distribution of singular values is similar to the system echo. But the magnitude and the steepness of the singular values, and the rank also give a certain difference between the sinusoidal frequency modulation interference and the system echo. Then we will analyze it by the theory of entropy, and use the entropy of singular spectrum to realize the distinction between system echo and interference signal.

B. INTERFERENCE RECOGNITION BASED ON SINGULAR SPECTRUM ENTROPY

Shannon entropy, also known as information entropy, is an effective index to quantitatively evaluate the degree of uncertainty of signal or system state. It can be combined with different signal processing methods to extract signal features in different transform spaces. The more concentrated the signal energy, the smaller the entropy value. Let $y = (y_1, y_2, \cdots y_n)$ be any random vector. If the probability of y_i occurrence is p_i, the Shannon entropy of y is defined as:

$$E_y = -\sum_{i=1}^{n} (p_i \log_2 p_i) \tag{19}$$

As discussed in Section III.A, the singular values of the trace matrix provide an inherent characteristic of the signal, especially for its stability and rotation invariance. As a combination of singular value decomposition and Shannon entropy, Singular spectral entropy benefits from their strengths and has impressive performances in signal information evaluation and information component analysis.

For a matrix A with singular values $\lambda_1, \lambda_2, \cdots, \lambda_L$ of matrix A, the probability p_i is defined as:

$$p_i = \frac{\lambda_i^2}{\sum_{i=1}^{m} \lambda_i^2} \tag{20}$$

Then, the singular spectral entropy of a given signal can be computed according to Eq. (19).

Since there are differences between the singular values of trace matrices of the echo and interference signals, the singular spectral entropy of them are also different. Although the singular spectral entropy of the echo signal and the interference signal will change with the change of relevant parameters, the change has a certain range, so the entropy of the singular spectrum can be used as an important parameter of interference recognition.

V. BISPECTRUM ANALYSIS

For the detection of the echo signal and the amplitude modulation interference signal, the singular spectral entropy can work well. However, for the sinusoidal frequency modulation interference signal, the value of the singular spectral entropy is similar to that of the detected echo, which is not conducive to the classification and recognition of these two signals. Next, we will introduce bispectrum analysis for further feature extraction.
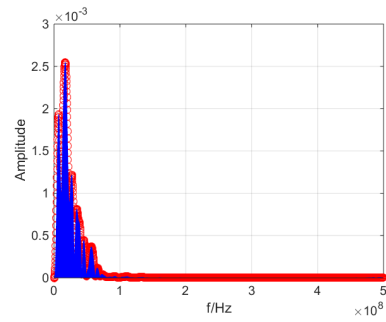

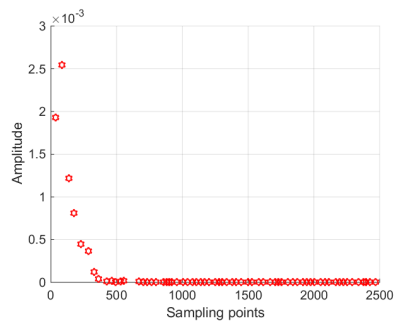**FIGURE 13.** The spike identification of detection echo bispectral slice.

FIGURE 14. The peak point of detection echo bispectral slice.

A. BISPECTRAL CONVEXITY ANALYSIS

Bispectrum is the generalization and development of power spectrum. Since phase information and amplitude information are preserved, the influence of Gaussian colored noise on non-Gaussian signals can be suppressed. It enjoys time invariance, scale invariance, phase retention and time independence. Therefore, it has been applied in many applications of signal processing [28]–[32].

Assuming the received signal satisfies a zero-mean stationary stochastic process, the bispectrum is defined as a third order cumulant Fourier transform, ie:

$$
\begin{aligned}
B_x(\omega_1, \omega_2) \\
= C_{3x}(\omega_1, \omega_2) \\
= \sum_{\tau_1=-\infty}^{+\infty} \sum_{\tau_2=-\infty}^{+\infty} c_{3x}(\tau_1, \tau_2) \exp\{-j(\omega_1\tau_1 + \omega_2\tau_2)\} \\
|\omega_1| \leq \pi, \quad |\omega_2| \leq \pi, \quad |\omega_1 + \omega_2| \leq \pi,
\end{aligned}
\tag{21}
$$

Due to the heavy computational burden of the bispectrum analysis, we use the diagonal slice of the bispectrum analysis for efficient calculation in the rest of this paper. According to the above definition, we perform bispectrum analysis on the detected echo and the two interference signals to obtain the peak spectrum of the bispectral slice, as shown in Fig. 13-18.

Next, we define the convexity T of the bispectral slice as follows:

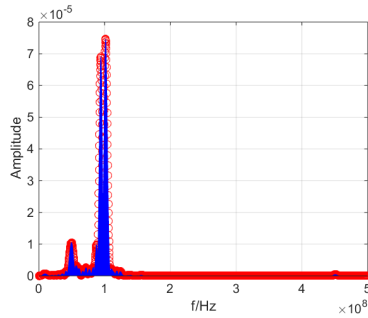$$T = \frac{\max(s(f_1, f_2))}{mean(s(f_1, f_2))} \tag{22}$$

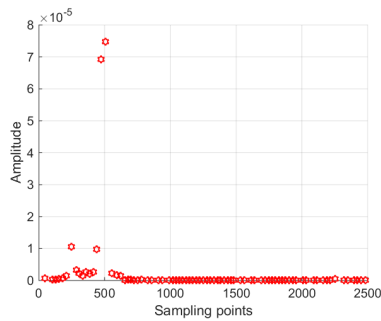**FIGURE 15.** The spike identification of sawtooth AM interference bispectral slice.

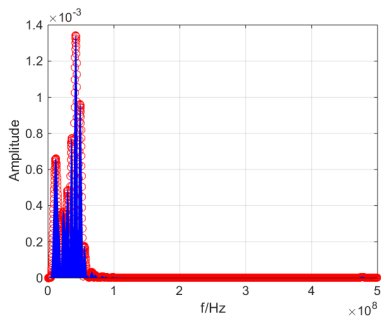**FIGURE 16.** The peak point of sawtooth AM interference bispectral slice.

FIGURE 17. The spike identification of sinusoidal FM interference bispectral slice.
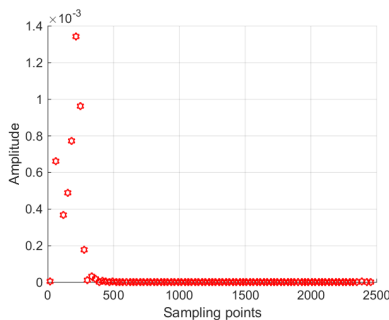

FIGURE 18. The peak point of sinusoidal FM interference bispectral slice.

where $s(f_1, f_2)$ represents the amplitude of the bispectral slice. The convexity T represents the ratio of the maximum value to the average level in the amplitude set. The greater the degree of convexity, the obvious ''heterogeneity'' exists in

the set; the smaller the convexity, the more averaged the level in the set, and the less prominent individuals. According to the above analysis of the bispectrum peak distribution, the convexity of a given signal is obtained as a feature of interference identification.

B. BISPECTRAL ENTROPY
According to the definition of singular spectral entropy in Section III.B, we define bispectral entropy in the same way.

For the peaks $s_1, s_2, \cdots, s_L$ of each peak point of the bispectral slice, the bispectrum peak point probability p_i is defined as:

$$p_i = \frac{s_i^2}{\sum_{i=1}^{m} s_i^2} \quad (23)$$

Then the expression of the bispectral entropy is given:

$$E_k = -\sum_{i=1}^{n} \left(\frac{s_i^2}{\sum_{i=1}^{m} s_i^2} \log_2 \frac{s_i^2}{\sum_{i=1}^{m} s_i^2} \right) \quad (24)$$

Based on the correlation parameters selected for solving the bispectral convexity, we calculate the peak entropy of the detected echo and the two kinds of interference, which is one of the basis for the classification and detection of the detected echo and the interference signal.

VI. GA-BP CLASSIFIER DESIGN
After establishing the feature parameter set, we select an appropriate classifier to identify echo and various types of interferences.

Genetic algorithm (GA) is an adaptive iterative optimization algorithm with good global search performance. Even if the defined fitness function is discontinuous and irregular, it can also find the overall optimal solution with great probability, and is suitable for parallel processing. The search does not depend on the characteristics of gradient information, and can be used to optimize the BP neural network [33]. The genetic algorithm is used to optimize the initial weight thresholds of a BP neural network, and search in a large range instead of the random selection of general initial weights. Then the BP algorithm is used to fine tune the network in this solution space to approximate optimal solution. The combination of GA and BP can exert the global search ability of the GA and the extensive nonlinear mapping ability of the BP neural network. Further, it can speed up the network training, improve the approximation ability and generalization ability in the whole learning process. Therefore, this paper constructs a GA-BP neural network to achieve classification of echo and interference.

GA-BP neural network is a multi-layer feedforward neural network based on GA. It has good nonlinear approximation ability, self-adaptive ability, robustness and fault tolerance [34], [35]. Moreover, it can optimize the weight and threshold of BP neural network by using the characteristics of
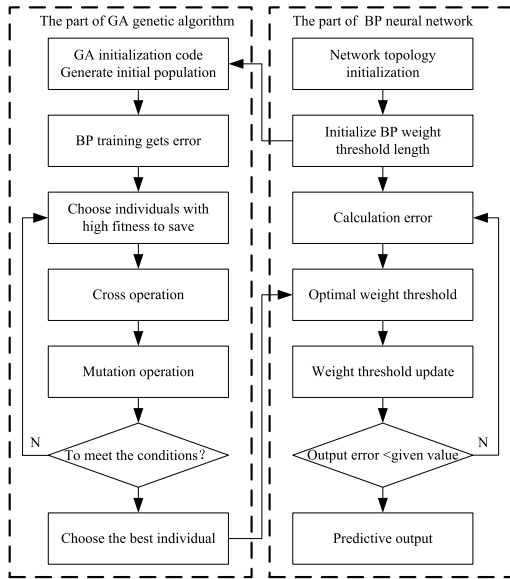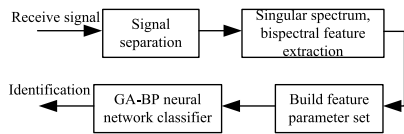
FIGURE 19. The flow of GA-BP algorithm.

FIGURE 20. Recognition model.

TABLE 2. The recognition rates of single feature quantity applied.

	Signal	Detection echo	Sawtooth AM interference	Sinusoidal FM interference
Recognition rate	Singular spectrum entropy	71.8	88.1	73.2
	Bispectral entropy	82.5	86.4	81.5
	Bispectral convexity	81.6	85.3	80.1

global search ability of GA. The classification algorithm of GA-BP neural network includes two parts: BP neural network part and GA optimization part. The algorithm flow is shown in Fig. 19.

The mathematical expression of the GA-BP algorithm is:

$$
\begin{cases}
E(v, w, \xi, \eta) = \dfrac{1}{M} \sum_{i=1}^{N} \sum_{t=1}^{m} [y_i(t) - \hat{y}_i(t)]^2 \\
\hat{y}_i(t) = f(\sum_{i=1}^{m} v_{it} g(\sum_{j=1}^{p} w_{ij} x_j(t) - \xi_i)) - \eta_t \\
\Delta w_{ij}(n) = -\eta g(n) + \beta \Delta w_{ij}(n-1) \\
t, w \in R^{m \times p}, \quad v \in R^{p \times n}, \quad \xi \in R^{p}, \quad \eta \in R^{n}
\end{cases}
\tag{25}
$$

where $E(v, w, \xi, \eta)$ is the sum of squared errors of BP neural network, N is the number of input and output samples of the network, $y_i(t)$ is the ideal output value of BP neural network training, and $\hat{y}_i(t)$ is the actual output value of BP neural network training. w_{ij}, v_{it} is the connection weight between nodes, ξ_i, η_t is the threshold; n is the iteration number; $g(n)$ is the corresponding weight gradient; f, g is the excitation function; β is the momentum factor; η is the adaptive learning rate; R is the matrix; $x_j(t)$ is normalized input parameters.

The echo signal and interference signal identification model is shown in Fig. 20.

In the experiment, the method of generating 500 sets of simulation data is: keep the chaotic sequence in the same way, the carrier frequency of the echo signal and the interference

signal is uniformly changed from 2GHz-7GHZ, and 500 sets of data are generated by simulation; the frequency of the modulated signal is uniformly changed from 2kHz-7kHz, and 500 sets of data are also generated by simulation; the bandwidth varies uniformly from 50MHz to 150MHz, and the simulation produces 500 sets of data. Then we randomly extracted 500 groups from the obtained 1500 sets of data as samples for the experiment. This not only ensures the uniform coverage of the relevant parameters, but also guarantees a certain randomness.

Through the simulation, 500 groups detection echo signal and the two different interference signals are tested, and 200 sets of data are randomly selected as the training data training network, and the remaining 300 sets of data are used as test data to test the network classification capabilities.

When the three characteristic parameters of bispectral entropy, bispectral convexity and singular spectrum entropy are used as the basis for feature discrimination, the recognition rates of echo and two kinds of interference are shown in Table 2.

Singular spectrum entropy is an indicator for evaluating the degree of uncertainty of signal singular value distribution. Since the echo and sinusoidal FM interference contain frequency modulation, it can be seen from Fig. 10-12 that the singular value distribution is more complex than the sawtooth AM interference. When singular spectrum entropy is used as the characteristic parameter for classification and recognition, the sawtooth AM interference is easier to be identified, the echo and sinusoidal FM interference is difficult to distinguish because of the singular spectrum entropy values are relatively close.

Bispectral convexity and bispectral entropy are both based on bispectrum analysis, which is an evaluation index of asymmetric and nonlinear characteristics of signals. Because the echo contains chaotic phase modulation and frequency modulation, it is a relatively complex nonlinear system, its bispectral structure is the most complicated, and the different of the peak point is obviously. Sinusoidal FM interference is a nonlinear frequency modulation, and the bispectral structure is relatively simple compared to echo. The sawtooth AM interference is linear amplitude modulation, the bispectral structure is the simplest among the three signals, and the number of slice peak points is the least. Due to the difference

TABLE 3. The recognition rates of echo and interference.

Signal	Detection echo	Sawtooth AM interference	Sinusoidal FM interference
Recognition rate	95.2	97.3	93.4

of bispectral structure, the classification of the echo and the two kinds of interference can be realized based on the bispectral convexity and the bispectral entropy. However, when the parameters of echo and interference are relatively close, the similarity and nonlinearity of the signal will be close, and the recognition rate will be reduced. So, it is necessary to cooperate with other parameters to realize classification and recognition of echo and interference.

When three characteristic parameters are used together as the basis for discrimination, the recognition rates of the echo and the two kinds of interference are as shown in Table 3.

Through simulation, the recognition accuracy of chaotic phase-modulated sawtooth frequency modulated echo can reach 95.2%, the recognition accuracy of sawtooth amplitude modulation interference can reach 97.3%, and the recognition accuracy of sinusoidal frequency modulation interference can reach 93.4%. Moreover, since the training process is completed in the early stage, the actual recognition process is short and the real-time performance is satisfactory.

VII. CONCLUSION

The CPLF-SrDS is introduced and analyzed. First, the separation of underdetermined echo and interference signal is realized by the method based on 4th-order cumulant and joint diagonalization. Then, for detecting echo signals, sinusoidal frequency modulation interference, sawtooth amplitude modulation interference, the paper proposes a method by using singular spectrum analysis and bispectrum analysis to analyze echo signals and interference signals, and extract feature parameters such as singular spectral entropy, bispectral slice convexity, and bispectral slice peak entropy. Finally, the GA-BP neural network is used to realize the classification of chaotic phase-modulated sawtooth frequency modulation echo signals, sawtooth amplitude modulation interference and sinusoidal frequency modulation interference, and to realize classification and identification between different interferences.

The method of underdetermined signal separation used in this paper has higher similarity between the recovered signal and the source signal than the current main research methods, especially at low signal-to-noise ratio. For the classification and identification of separated signals, the traditional methods mostly focus on the analysis of the signal itself and the signal spectrum, and cannot better mine the deep features of the signal. When the signal is more complex or the similarity is higher, the traditional method is difficult to classify. In this paper, the method of bispectrum analysis and singular spectrum analysis is proposed. The feature parameters of echo and interference signals are extracted for signal identification.

This method adopts the theory of signal spectrum analysis to better explore the deep features of the signal. For the characteristic parameters proposed in the paper, we use a BP algorithm based on genetic algorithm improvement. This algorithm optimizes the threshold of BP network by genetic algorithm. Compared with traditional neural network algorithm, the classification recognition is higher.

REFERENCES

[1] X. Guoxin, T. Xin, P. Wei, and R. Tao, "Clustering analysis based on chaos micro variation adaptive genetic algorithm for radio fuze jamming," in *Proc. Control Decis. Conf.*, 2017, pp. 616–620.

[2] Y. Huang, X.-H. Hao, Z.-J. Kong, and B. Zhang, "Recognition of target and jamming signal for FM fuze based on entropy features," *Acta Armamentarii*, vol. 38, no. 2, pp. 254–260, 2017.

[3] H. Yuan and J. Sui, "Jamming based on digital jamming synthesis against pseudo random code phase modulation fuze," *J. THz Sci. Electron. Inf. Technol.*, vol. 14, no. 1, pp. 64–67, 2016.

[4] T. Benren, "An ECCM model technical development trends to the demands of the future EW combat," *IEEE Aerosp. Electron. Syst. Mag.*, vol. 9, no. 6, pp. 12–16, Jun. 1994.

[5] Y. A. N. Hai, L. I. Guo-Hui, and L. I. Jianxun, "Signal feature extraction methods of radar anti-deception jamming," *J. Univ. Electron. Sci. Technol. China.*, vol. 44, no. 1, pp. 50–54, 2015.

[6] M. Niknazar, H. Becker, C. Jutten, B. Rivet, and P. Comon, "Blind source separation of underdetermined mixtures of event-related sources," *Signal Process.*, vol. 101, no. 8, pp. 52–64, 2014.

[7] Y. Li, A. Cichocki, and S.-I. Amari, "Analysis of sparse representation and blind source separation," *Neural Comput.*, vol. 16, no. 6, pp. 1193–1234, 2004.

[8] T. Higuchi, N. Takamune, T. Nakamura, and H. Kameoka, "Underdetermined blind separation and tracking of moving source based on DOA-HMM," in *Proc. IEEE Int. Conf. Acoust., Speech Signal Process. (ICASSP)*, May 2014, pp. 3191–3195.

[9] N. Tengtrairat and W. L. Woo, "Single-channel separation using underdetermined blind autoregressive model and least absolute deviation," *Neurocomputing*, vol. 147, no. 1, pp. 412–425, 2015.

[10] O. S. Alshabrawy and A. E. Hassanien, "Underdetermined blind separation of mixtures of an unknown number of sources with additive white and pink noises," in *Proc. 5th Int. Conf. Innov. Bio-Inspired Comput. Appl. (IBICA)*, in Advances in Intelligent Systems and Computing, vol. 303, 2014, pp. 241–250.

[11] A. Aissa-El-Bey, N. Linh-Trung, K. Abed-Meraim, A. Belouchrani, and Y. Grenier, "Underdetermined blind separation of nondisjoint sources in the time-frequency domain," *IEEE Trans. Signal Process.*, vol. 55, no. 3, pp. 897–907, Mar. 2007.

[12] H. C. Zhao and X. G. Zhou, "Anti-jamming performance evaluation of linear frequency-modulated continuous wave fuze based on ambiguity function incision," *Acta Armamentarii*, vol. 30, no. 12, pp. 1591–1595, 2009.

[13] X. G. Zhou *et al.*, "Performance analysis concerning anti-noise for pseudo-random code phase modulation and pulse amplitude modulation combined fuze based on Doppler effect," *J. Electron. Inf. Technol.*, vol. 30, no. 8, pp. 1874–1877, 2008.

[14] J. B. Liu, H. C. Zhao, and J. W. Lu, "Performance analysis concerning antinoise for several pseudo-random code fuzes," *Acta Armamentarii*, vol. 26, no. 1, pp. 20–24, 2005.

[15] Y. Yan and Z.-Z. Cui, "Anti-jamming performance of ultra wideband radio fuze," *Acta Armamentarii*, vol. 31, no. 1, pp. 13–17, 2010.

[16] Z. Li, P. Li, X.-H. Hao, and X. P. Yan, "Anti-active noise jamming performance of pulse Doppler fuze," *Acta Armamentarii*, vol. 6, no. 6, pp. 1001–1008, 2015.

[17] Y. Lu, M. Li, H. Chen, Z. Wang, and L. Zuo, "Countering DRFM range gate pull-off jamming based on singular spectrum analysis," *J. Electron. Inf. Technol.*, vol. 38, no. 3, pp. 600–606, 2016.

[18] X. Wang, Y. Zhou, Z. Chen, and D. Zhou, "Research on low probability of intercept radar signal recognition using deep belief network and bispectra diagonal slice," *J. Electron. Inf. Technol.*, vol. 38, no. 11, pp. 2973–2976, 2016.
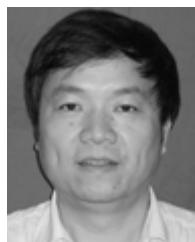
[19] J. Zabalza, J. Ren, Z. Wang, S. Marshall, and J. Wang, "Singular spectrum analysis for effective feature extraction in hyperspectral imaging," *IEEE Geosci. Remote Sens. Lett.*, vol. 11, no. 11, pp. 1886–1890, Nov. 2014.

[20] L. De Lathauwer, J. Castaing, and J.-F. Cardoso, "Fourth-order cumulant-based blind identification of underdetermined mixtures," *IEEE Trans. Signal Process.*, vol. 55, no. 6, pp. 2965–2973, Jun. 2007.

[21] S. N. Ge and M. Han, "Fourth-order cumulant of tensor decomposition method for blind identification of underdetermined separation," *Acta Electron. Sinica*, vol. 42, no. 5, pp. 992–997, 2014.

[22] H. J. Yu and D. S. Huang, "Graphical representation for DNA sequences via joint diagonalization of matrix pencil," *IEEE J. Biomed. Health Inform.*, vol. 17, no. 3, pp. 503–511, May 2013.

[23] M. Congedo, C. Gouy-Pailler, and C. Jutten, "On the blind source separation of human electroencephalogram by approximate joint diagonalization of second order statistics," *Clin. Neurophysiol.*, vol. 119, no. 12, pp. 2677–2686, 2008.

[24] A. Ziehe, P. Laskov, G. Nolte, and K.-R. Müller, "A fast algorithm for joint diagonalization with non-orthogonal transformations and its application to blind source separation," *J. Mach. Learn. Res.*, vol. 5, pp. 777–800, Jul. 2004.

[25] W. Fuxiang, L. Zhongkan, and Z. Jun, "A new joint diagonalization algorithm with application in blind source separation," *IEEE Signal Process. Lett.*, vol. 13, no. 1, pp. 41–44, Jan. 2006.

[26] C. Yi, Y. Lv, Z. Dang, H. Xiao, and X. Yu, "Quaternion singular spectrum analysis using convex optimization and its application to fault diagnosis of rolling bearing," *Measurement*, vol. 103, pp. 321–332, Jun. 2017.

[27] Y. Lu and S. Li , "CFAR detection of DRFM deception jamming based on singular spectrum analysis," in *Proc. IEEE Int. Conf. Signal Process.*, Oct. 2018, pp. 1–6.

[28] C. Liu and X. Wu, "Arbitrarily high-order time-stepping schemes based on the operator spectrum theory for high-dimensional nonlinear Klein–Gordon equations," *J. Comput. Phys.*, vol. 340, pp. 243–275, Jul. 2017.

[29] S. Yang, B. Tian, and R. Zhou, "A jamming identification method against radar deception based on bispectrum analysis and fractal dimension," *J. Xian Jiaotong Univ.*, vol. 50, no. 12, pp. 128–135, 2016.

[30] X. Chen, X. Zhu, and D. Zhang, "A discriminant bispectrum feature for surface electromyogram signal classification," *Med. Eng. Phys.*, vol. 32, no. 2, pp. 126–135, 2010.

[31] M. Shiraishi, D. Nitta, S. Yokoyama, K. Ichiki, and K. Takahashi, "CMB bispectrum from primordial scalar, vector and tensor non-Gaussianities," *Prog. Theor. Phys.*, vol. 125, no. 4, pp. 795–813, 2011.

[32] S. Guoji, S. McLaughlin, X. Yongcheng, and P. White, "Theoretical and experimental analysis of bispectrum of vibration signals for fault diagnosis of gears," *Mech. Syst. Signal Process.*, vol. 43, nos. 1–2, pp. 76–78, 2014.

[33] Z. C. Qiu, W. M. Zhang, Y. Guo, J. Liu, and M. M. Cheng, "Evaluation on quantitative recognition of micro cracks by magnetic leakage test based on GA-BP neural network," *Nondestruct. Test.*, vol. 38, no. 2, pp. 1–4, 2016.

[34] Y. Yang, G. Wang, and Y. Yang, "Parameters optimization of polygonal fuzzy neural networks based on GA-BP hybrid algorithm," *Int. J. Mach. Learn. Cybern.*, vol. 5, no. 5, pp. 815–822, 2014.

[35] H. Q. Yu, Z. Liu, and Q. H. Tian, "Spectral characterization model of liquid crystal display based on GA-BP neural network and PCA," *Chin. J. Liquid Cryst. Displays*, vol. 31, no. 2, pp. 201–207, 2016.

DONGXU WEI was born in Huai'an, Jiangsu, China, in 1982. He received the master's degree from the College of Automation Engineering, Nanjing University of Aeronautics and Astronautics, Nanjing, China, in 2007. He is currently pursuing the Ph.D. degree with the School of Electronic and Optical Engineering, Nanjing University of Science and Technology, Nanjing. He is currently with the School of Physics and Electronic Electrical Engineering, Huaiyin Normal University, and Jiangsu Province Key Construction Laboratory of Modern Measurement Technology and Intelligent System. His current research interests include tensor decomposition, radar fuze, and robot for intelligent welding.

SHUNING ZHANG was born in Weihai, China, in 1977. She received the Ph.D. degree in signal and information processing from the Nanjing University of Science and Technology, in 2006, where she is currently a Professor with the School of Electronic and Optical Engineering. Her research interests include non-stationary signal processing, parameters extraction, and multi-fractional signal analysis.

SI CHEN was born in Xuancheng, Anhui, China, in 1988. He received the B.S. and M.S. degrees in communication and information engineering from the Nanjing University of Science and Technology, Nanjing, China, in 2010 and 2015, respectively, where he is currently an Associate Professor with the School of Electronic and Optical Engineering. His research interests include missile-borne SAR imaging, moving target detection, and digital signal processing.

HUICHANG ZHAO was born Wenzhou, China, in 1958. He is currently a Professor with the School of Electronic and Optical Engineering, Nanjing University of Science and Technology. His current research interests include signal processing and the theories and methods of modern electronic countermeasures.

LINGZHI ZHU was born in Rugao, Jiangsu, China, in 1994. He received the B.S. degree in electronic engineering from the Nanjing University of Science and Technology, Nanjing, China, in 2016, where he is currently pursuing the Ph.D. degree in electronic and optical engineering. His research interests include radar micro-doppler and digital signal processing.

• • •